

Prediction of the Conditional Probability Densities of Time Interval Extrema with Application to Risk-Sensitive Scheduling^{*,**}

Buyi Yu^{a,*}, Wenyan Tang^a

^a*Campus Box 7571, North Carolina State University, Raleigh, NC 27695, United States*

Abstract

Planning and scheduling activities in the electrical power system, such as the commitment of reserve generation, often involve the statistical characterization of peak demand. Due to the stationarity assumption of classical extreme value analysis (EVA), existing approaches in the industry apply EVA on simulated annual peaks created by weather-dependent surrogate models using Monté-Carlo simulations on a per-scenario basis. In day-ahead scheduling, the daily peak demand changes upon various factors besides temperature, Monté-Carlo experiments become intractable, and state-of-the-art generalized additive model for location, scale and shape (GAMLSS)-based nonstationary EVA is often impractical due to convergence issues on high-dimensional covariates. This article explores uncharted territories and proposes a novel nonstationary EVA estimator that predicts the probable peaks of high-resolution time intervals and their corresponding conditional probability densities based on calendar information and weather conditions where historical peaks are observed. Compared to GAMLSS, our method automatically discovers and robustly models complex relationships between the covariate and the peak demand density. We present a case study on the determination of day-ahead scheduling capacity and demonstrate that compared to the industry approach, our approach results in a 38% reduction in the yearly total committed capacity while maintaining the given risk requirement.

Keywords: Risk-averse unit commitment, extreme value analysis, ensemble model, estimation theory, probabilistic regression, energy market

*This paper is partly derived from the work supported by the U.S. Department of Energy's Office of Energy Efficiency and Renewable Energy (EERE) through the Solar Energy Technology Office (SETO) under Award DE-EE0009357. The funding source has no involvement in the development of the methodology, design, preparation, or interpretation of the case study, or the decision to submit for publication.

**Source code artifacts are available in repository <https://github.com/byu9/extreme-tree>. Results in the paper correspond to revision 6e80006.

*Corresponding author

Email addresses: byu9@ncsu.edu (Buyi Yu), wtang8@ncsu.edu (Wenyan Tang)

1. Introduction

Increasingly frequent extreme weather events, such as the winter storm that resulted in the 2021 Texas power crisis, can disrupt power balance, leading to cascading failures of the power grid with devastating and sustained impacts [1]. From long-term planning to intra-hour real-time operation, rigorous efforts are dedicated to characterizing extreme capacity shortage events and the statistical analysis from which resource adequacy requirements are partly determined. For example, according to the 2016 technical guideline document [2], the North American Electric Reliability Corporation (NERC) leverages cost-effectiveness against risk acceptability and performs annual probabilistic assessments that cover worst-case probabilistic evaluations of generation outages, transmission contingencies, availability of renewable and demand-side management (DSM) resources, and demand uncertainty. In the ISO New England 2027 winter study [3], probabilistic extrema analysis is utilized to identify high-risk weather scenarios that may result in severe energy shortfalls. Probabilistic predictions of generation deficits in the form of survival functions and probability density functions (PDFs) have also been introduced as stochastic risk control constraints [4] [5]. Under increasing penetration of utility-scale and behind-the-meter variable renewable resources, literature on energy forecasting indicates recognition of the practicality of probabilistic predictions, also known as full-distribution metrics, in mitigation of the effects of resource intermittency and variability to system operations [6, 7, 8].

1.1. *Characteristic and requirements of risk-sensitive scheduling*

Secure power system operations must compensate for generator outages, demand fluctuations, and the uncertainty of increasingly common renewable energy systems. We use risk-sensitive scheduling to refer to operator decisions that explicitly account for the risk of high-impact events characterized by their probability and severity using statistical methods. Such decisions straddle the balance between the increased cost of resource over-commitment, which results in waste of natural resources, and the consequence of under-commitment, such as the societal impact of blackouts.

Contrary to economic unit commitment, which bases decisions on the typical demand, risk-sensitive security-constrained unit commitment decisions include modeling of the peak demand since system failures are caused by extremes. Given the ethical responsibility of the system operator as a regulated monopoly entrusted with a mission-critical infrastructure, energy regulatory and oversight agencies create stringent reliability guidelines to enforce accountability, and these guidelines are often given in terms of probabilistic measures formulated on the statistical behavior of peak demand. For example, in North America, NERC standard BAL-502-RF-03 [9] specifies reliability requirement in terms of loss-of-load probability (LOLP), defined as the probability that the demand exceeds available generation capacity; in Australia, the Australian Energy Market Operator (AEMO) specifies reliability requirement in National Electricity Law [10] in terms of expected unserved energy (EUE), also known simply as

the unserved energy (USE) or expected energy not served (EENS), defined as the statistical expectation of the amount of energy the system cannot serve due to demand exceeding capacity, often given in percentage of annual total energy served; in the European Union, the regulation (EU) 2019/943 [11] demands transparency and regular monitoring of the EUE and loss-of-load expectation (LOLE), defined as the statistical expectation of the number of time intervals in which the demand exceeds available generation capacity.

While the aforementioned regulatory risk metrics currently only apply to annual time intervals, our approach provides the necessary means to model risk in much shorter intervals to allow fine-grained control. This capability is increasingly important for the management of short-term intermittency and volatility of high-penetration renewable energy systems.

1.2. Challenges with existing forecasting approaches

Probabilistic regression is a method that estimates likelihoods from deterministic observations. In parametric probabilistic regression, the probable outcome $y(\mathbf{x})$ under the condition known as the covariate \mathbf{x} is assumed to follow a predetermined distribution family $D(\hat{\theta}(\mathbf{x}))$ with predicted deterministic parameter $\hat{\theta}(\mathbf{x})$. In non-parametric probabilistic regression, the density does not assume a predetermined form. Compared to parametric probabilistic regression, non-parametric probabilistic regression is largely assumption-free and excels at prediction tasks where the distribution family is unknown, while parametric probabilistic regression requires the establishment of statistical assumptions that may be unsupported by observational evidence.

Popular non-parametric probabilistic regression methods, such as the well-known quantile regression (QR) [12] and recent artificial neural network (ANN)-based quantile forecasting methods such as convolution neural network (CNN) [13], attentive quantile temporal convolution neural network (QTCN) [14], and deep reinforcement learning [15] produce estimates of the quantile function (QF), also known as the inverse cumulative distribution function (CDF) on a set of quantiles. Despite their popularity, quantile forecasting methods have several notable shortcomings. First, they tend to suffer from quantile crossover [16], referring to the phenomenon that the approximated inverse CDF is not in a monotonically non-decreasing form, implying the existence of unsubstantial negative densities. Second, quantile forecasting methods produce discrete estimates of the probability density on a limited set of quantiles. To obtain a continuous density that can be adopted by stochastic optimal scheduling problems utilizing gradient-based optimization, the predicted quantiles must undergo post-processing such as kernel density estimation (KDE) [17] to interpolate the missing quantiles. Last, as we will demonstrate through an experiment later in this paper, due to the rarity of observations at extreme quantiles, quantile forecasting methods are unable to approximate the probability density of low-probability high-consequence (LPHC) events, also known as “black swan” events.

As an alternative to non-parametric methods, parametric probabilistic regression methods such as generalized autoregressive conditional heteroskedasticity (GARCH) [18, 19] and GAMLSS [20] have been proposed. While GARCH can model nonstationarity of the variance, also known as the second moment, GAMLSS can account for the nonstationarity of the location, scale, and shape parameters by modeling them as functions of the covariate using explicit formulas or spline approximations. However, existing literature such as [21] has described GAMLSS to struggle with high-dimensional covariates, and in our case study in Section 5, GAMLSS failed to converge.

1.3. Accurately estimating the density of extreme values

Time series often contain far more ordinary observations than extreme observations. As a result, regardless of parametric or non-parametric probabilistic regression, directly estimating the probability density of rare occurrences, although straightforward, does not provide well-calibrated density estimates of the outliers and tends to bias towards the accuracy of the inliers. The density of extrema can be approximated more accurately if the time series only contains extreme observations, which can be obtained using two common approaches. The block maxima approach divides a high-resolution time series into lower-resolution and non-overlapping time intervals, each containing a relatively large number of observations, before taking the maximum of each interval. Alternatively, the points-over-threshold approach retains extreme observations above a threshold and drops all other observations. The block minima and points-under-threshold can be obtained in similar ways.

EVA is a mature branch of statistics that studies the accurate modeling of the probability density of the outliers of various statistical distributions and has been the cornerstone in the prediction of rare natural disasters such as fire, flood, and earthquake, reliability studies of materials and aerospace equipment, and finance [22]. It has been discovered that as the block size increases, if the block maxima of independently and identically distributed (i.i.d.) observations of an unknown distribution converge, it will approach asymptotically to the generalized extreme value distribution (GEV). Similarly, as the threshold increases, if the distribution of points-over-threshold converges, it will approach asymptotically to the generalized Pareto distribution (GPD). Due to symmetry, the same phenomenon is demonstrated on the block minima and points-under-threshold and applies to sign-opposite transformations of the GEV and GPD. Despite the lack of observations at extreme quantiles, given a sufficient block size or threshold, the probability density of extrema can be accurately predicted in the form of GEV or GPD.

While GEV or GPD used in other engineering fields often model some form of nonstationarity in the location and scale parameters, fitting of nonstationary models often involves manual selection of trend models [23]. In the case of GEV, the shape parameter is considered to be more difficult to estimate, and engineering methods tend to assume a constant shape parameter [24, 25]. The method proposed herein can automatically discover the potentially nonlinear re-

relationship between a high-dimensional covariate and all three GEV parameters, including the shape.

1.4. Reconciling diverging trends in forecasting research and the industry

Despite risk management concentrating on controlling the occurrence and reducing the severity of the worst case, recent literature tends to favor quantile forecasting methods, which are typically optimized for overall performance, overlooking the rare extremes where critical system risks lie. A recent report from the industry [26] signaled improved probabilistic modeling as one of the critical forward-facing issues in ensuring reliability. Whereas classical EVA is the canonical approach in extreme value probabilistic assessments, it assumes stationarity and cannot model the effect of external factors on the estimated density, preventing the adoption of classical EVA in high-resolution applications such as day-ahead scheduling, whereas the state-of-the-art GAMLSS is often impractical due to the aforementioned convergence issues. Leveraging established machine learning techniques and EVA, the paper proposes a novel method to model and predict peak demand uncertainty. The objectives of this paper are as follows:

- To develop a widely applicable conditional parametric density model for time series extrema that surpasses quantile-based models in accurately modeling “black swan” events.
- To propose a novel nonstationary EVA estimator based on the proposed density model and overcome the stationarity limitation of classical EVA and the convergence issue of GAMLSS.
- To apply nonstationary EVA in high-resolution risk-sensitive scheduling applications in the power system.

While many existing forecasting methods, such as the aforementioned deep learning methods [13, 14, 15], focus on predicting point values or quantiles, our approach aims to estimate the conditional distribution of peak demand using an EVA framework. We use Table 1 to summarize the key differences that distinguish our method from a large portion of existing forecasting literature.

Aspect	Existing methods	Proposed method
Prediction format	Series of mean or quantiles	Series of probability densities
Forecasting target	Ordinary and peak values	Only peak densities
Accuracy of peaks	Often overlooked	Specifically targeted
Assumptions	Often empirical	Conditional EVA framework
Reliability metrics	Often limited to quantiles	VaR, CVaR, EUE, LOLP

Table 1: Key differences that distinguish our method from existing forecasting literature. EVA—extreme value analysis, VaR—value-at-risk, CVaR—conditional value-at-risk, EUE—expected unserved energy, LOLP—loss-of-load probability.

1.5. Key contributions and paper structure

The key contributions of this paper are, first, the formulation of a rigorous statistical framework to model nonstationary time series extrema, second, a novel nonstationary EVA approach to estimate GEV parameters under the proposed framework, and finally, a case study that demonstrates a realistic use case of the proposed approach. The structure of the paper and minor contributions are as follows:

- In the next section, we describe the problem, formulate the conditional framework to model nonstationary extrema densities, elucidate the assumptions, investigate the conditions for the weakening of the framework, and present two configurations to model autocorrelation.
- In Section 3, we conceive and expound a novel nonstationary EVA approach, compare two estimation methods, justify the selection, and elaborate on the step-by-step operation of the algorithm and its termination.
- In Section 4, through an experiment, we contrast our approach with a theoretically most efficient estimator, juxtapose it with two competitors, scrutinize the results, and corroborate the superiority of our approach.
- In Section 5, through a case study, we integrate our approach with a real-world application, augment existing industry practices, and assess the benefits of risk management and cost reduction.

Given potential criticisms regarding the lack of deep learning in the proposed approach, we acknowledge that deep learning models, such as long short-term memory (LSTM) networks [27] or temporal convolutional networks [28], can be highly effective at capturing long-term dependencies in time series data. However, the objective of this paper is not to propose yet another deep-learning method on the well-studied topic of deterministic regression, but rather a novel probabilistic regression method that estimates the time-varying probability densities of peak demand using a structured EVA framework. While we considered deep learning during the design of our method, it is not naturally aligned with established EVA estimators. We view the integration of deep learning as an interesting direction for future exploration, but not as a necessary condition for establishing the value and practicality of our method in its current form.

2. Problem statement

For deterministic sub-interval condition \mathbf{x} , we use symbol \mathcal{Y} to represent the event that the peak demand of the enclosing interval is observed at \mathbf{x} . Given the knowledge that event \mathcal{Y} occurs, our goal is to predict the distribution of the peak demand $\Pr(y|\mathcal{Y}, \mathbf{x})$ based on future environmental condition \mathbf{x} , which is also known and deterministic. The phrase “peak demand” implies that it is an observation that belongs to a time interval. The relationship between sub-interval observations, intervals, and interval maxima is illustrated in Fig. 1.

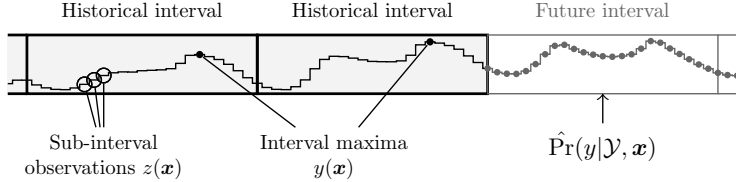


Figure 1: Sub-interval observations, interval maxima, and the predicted conditional probability density of the interval maximum.

Using $\Pr(\mathcal{Y}|\mathbf{x})$ to represent the probability of sub-interval condition \mathbf{x} resulting in peak demand event \mathcal{Y} , the joint probability $\Pr(y, \mathcal{Y}|\mathbf{x})$ of peak demand event \mathcal{Y} of severity y occurring under sub-interval condition \mathbf{x} is given by

$$\Pr(y, \mathcal{Y}|\mathbf{x}) = \Pr(y|\mathcal{Y}, \mathbf{x}) \Pr(\mathcal{Y}|\mathbf{x}). \quad (1)$$

While it is known as a rule-of-thumb that daily peaks tend to be observed under hot weather and in the afternoon, estimation of peak demand event frequency $\Pr(\mathcal{Y}|\mathbf{x})$ is beyond the scope of this paper. When $\Pr(\mathcal{Y}|\mathbf{x})$ is unknown, in risk management it is prudent to assume the worst-case using $\Pr(\mathcal{Y}|\mathbf{x}) \equiv 1$, where peak demand events are assumed to always occur at every sub-interval and our predictions $\hat{\Pr}(y|\mathcal{Y}, \mathbf{x})$ directly yields the response joint distribution $\Pr(y, \mathcal{Y}|\mathbf{x})$. The identity eq. (1) may invoke the context of a Bayesian method and create an impression of attempts to conceal its flaws. We therefore wish to emphasize that the method introduced herein is not a Bayesian method, eq. (1) is always evaluated from right to left, and we do not use Bayes' rule to find the probability of a cause given its effect. The choice of applying $\Pr(\mathcal{Y}|\mathbf{x}) \equiv 1$ is justified as described.

A typical application of our approach is shown in Fig. 2. The covariates exemplified in the artwork reflect common types of elements often chosen in time-series forecasting, and the actual covariate structure is application-specific and informed by domain knowledge. We invite the reader to skip ahead to the case study in Section 5, which demonstrates the choice of covariate for a real-world application. For the set of covariate dimensions \mathcal{M} , set of hourly intervals \mathcal{N} , and supplied covariate $\mathbf{x}_{\mathcal{M}, \mathcal{N}}$ corresponding to hourly conditions, we produce estimates of the conditional daily peak distribution $\hat{\Pr}(y|\mathcal{Y}, \mathbf{x}) = \text{GEV}(\hat{\boldsymbol{\theta}}|\mathbf{x})$ at every hour.

2.1. Conditional framework for nonstationary extreme value densities

For unknown initial distribution $D(\mathbf{x})$ that may change with covariate \mathbf{x} , sub-interval observations $z(\mathbf{x})$ under condition of \mathbf{x} are assumed to be i.i.d. realizations of the following stochastic process:

$$z(\mathbf{x}) \sim D(\mathbf{x}) \quad (2)$$

For the block maxima $y(\mathbf{x}) = \max(z_1, \dots, z_M|\mathbf{x})$ of M i.i.d. observations, according to the Fisher-Tippett-Gnedenko theorem, if as $M \rightarrow \infty$ the distribution of $y(\mathbf{x})$ is non-degenerate, it is well approximated by the GEV, regardless of

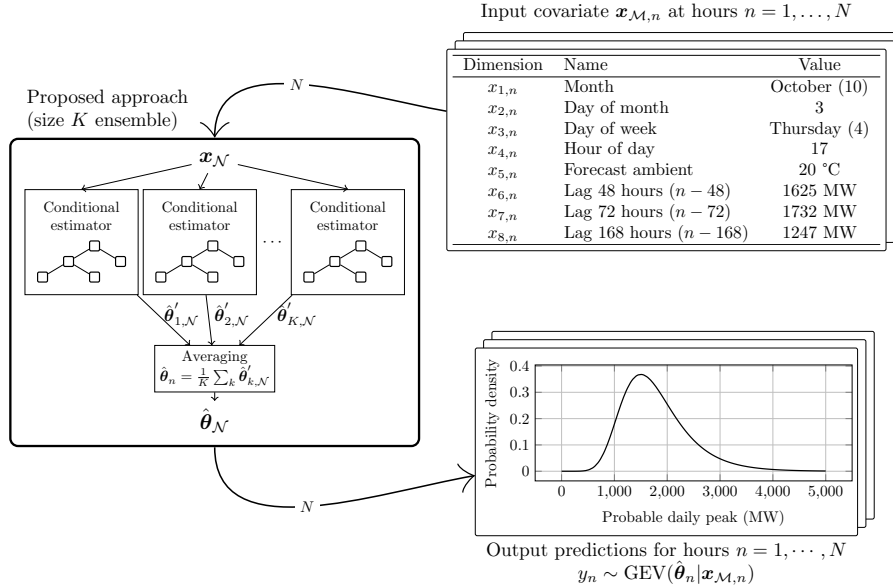


Figure 2: Example use case. The predictions are in the form of conditional daily peak distribution $y \sim \text{GEV}(\hat{\theta}|\mathbf{x})$ that is updated at every hour. The covariate elements and results in the artwork are examples intended to illustrate the mechanics of our method and not to be taken as prescriptive implementation advice. GEV—generalized extreme value distribution.

the initial distribution $D(\mathbf{x})$. The domain of attraction (DOA) refers to the set of initial distributions whose block maxima can be approximated by GEV. For $p_1, \dots, p_4 \in (0, 1)$, the necessary and sufficient condition for initial distribution D with inverse CDF $F^{-1}(z)$ to belong to the DOA is [29]:

$$\lim_{M \rightarrow \infty} \frac{F^{-1}(p_1^{1/M}) - F^{-1}(p_2^{1/M})}{F^{-1}(p_3^{1/M}) - F^{-1}(p_4^{1/M})} = \frac{(-\log p_1)^{-\xi} - (-\log p_2)^{-\xi}}{(-\log p_3)^{-\xi} - (-\log p_4)^{-\xi}} \quad (3)$$

The DOA of GEV encompasses a wide range of initial distribution families, making the statistical framework widely applicable. In general, block maxima of initial distributions with exponentially or sub-exponentially decaying upper tails, such as normal, exponential, log-normal, Gamma, and Rayleigh, converge to the type-I GEV known as Gumbel, where $\xi = 0$, those with polynomial decaying upper tails such as Cauchy, Pareto, and Student's t converge to the type-II GEV known as Fréchet, where $\xi > 0$, and those with a finite upper bound, such as uniform or beta, converge to the type-III GEV known as inverse Weibull, where $\xi < 0$.

For probable outcome y , location $\mu \in \mathbb{R}$, scale $\sigma > 0$, and shape $\xi \in \mathbb{R}$, the support of GEV refers to y that satisfies $1 + \xi \left(\frac{y - \mu}{\sigma} \right) > 0$. The PDF of the GEV

is given by

$$\Pr_{\text{GEV}}(y; \mu, \sigma, \xi) = \frac{1}{\sigma} \tau^{1+\xi} \exp(-\tau), \quad (4)$$

where

$$\tau(y; \mu, \sigma, \xi) = \begin{cases} (1 + \xi \frac{y-\mu}{\sigma})^{-\frac{1}{\xi}} & \xi \neq 0, \\ \exp(-\frac{y-\mu}{\sigma}) & \xi = 0. \end{cases} \quad (5)$$

When the block size M is sufficiently large, the block maxima and minima can be modeled by

$$y^{\text{MAX}}(\mathbf{x}) \sim \text{GEV}(\mu^{\text{MAX}}, \sigma^{\text{MAX}}, \xi^{\text{MAX}} | \mathbf{x}), \quad (6a)$$

$$-y^{\text{MIN}}(\mathbf{x}) \sim \text{GEV}(-\mu^{\text{MIN}}, \sigma^{\text{MIN}}, \xi^{\text{MIN}} | \mathbf{x}), \quad (6b)$$

where

$$y^{\text{MAX}}(\mathbf{x}) = \max(z_1, \dots, z_K | \mathbf{x}), \quad (7a)$$

$$y^{\text{MIN}}(\mathbf{x}) = \min(z_1, \dots, z_K | \mathbf{x}). \quad (7b)$$

2.2. Addressing autocorrelation

When improperly modeled, autocorrelation in time series results in the weakening of the proposed framework due to violation of the i.i.d. assumption eq. (2). As discussed in [30], GEV is still applicable under weak autocorrelation as long as the block maxima are effectively independent. Furthermore, it is theoretically proven in [31] that even with relatively strong autocorrelation with a slow rate of decay of the autocorrelation function (ACF), the classical asymptotic behavior of EVA still holds. For example, GEV can be applied to predict the probability of extreme floods in hydrology based on monthly rainfall maxima, despite the month-to-month correlation. Examples of EVA being applied to potentially weakly autocorrelated series in power system applications include [32], where autocorrelation in the ramp rate is reduced due to differencing, and [33], where the peaks are effectively independent. We argue that the conditional EVA framework we established in eq. (6) is still applicable under strong autocorrelation using either of the following configurations:

- Direct modeling of autocorrelation: For vector $\mathbf{z}_{<n} = [z_{n-r}, \dots, z_{n-2}, z_{n-1}]^T$ representing the history of z_n up to lag order r , assuming that strongly correlated lag orders are included in $\mathbf{z}_{<n}$, for exogenous factors $\boldsymbol{\psi}_n$, an autoregressive nonstationary process can be approximated as locally i.i.d. using the unknown conditional distribution $z_n \sim D(z | \boldsymbol{\psi}_n, \mathbf{z}_{<n})$, which is in the form of eq. (2). An example of this configuration is shown in Fig. 2, where the predicted daily peak distribution is conditioned on strongly correlated historical demand.
- Delegated modeling of autocorrelation: For \hat{z}_n representing the forecast produced by a base regression model known as the delegate, given the assumption that the residuals of such model are non-autocorrelated, for

exogenous factors ψ_n , an autoregressive nonstationary process can be approximated as locally i.i.d. using the unknown conditional distribution $z_n \sim D(z|\psi_n, \hat{z}_n)$, which is in the form of eq. (2). This configuration is recommended when the delegate is already highly accurate, allowing our approach to take advantage of the delegate when creating the peak demand probabilistic forecast. An example of this configuration is the PJM case study in Section 5.

We will demonstrate through the case study in Section 5 that under worst-case baseline probability, this conditional EVA framework allows us to calculate the exact amount of required day-ahead capacity to satisfy a given risk requirement and, compared to annual EVA assessments, prevents over-commitment of generation resources and can potentially lead to a significant reduction of wholesale electricity prices.

3. Methodology

Contrary to single-valued forecasting approaches such as least-squares regression, which aims to minimize the mean squared error (MSE) of predictions against the corresponding targets, given a set of historical conditions and block maxima in the form of covariate–target pairs $(\mathbf{x}_{\mathcal{M}\mathcal{N}}, y_{\mathcal{N}})$, the objective of the proposed approach is to predict the parameters of the conditional distribution $\text{GEV}(\hat{\boldsymbol{\theta}}_{\mathcal{N}}|\mathbf{x}_{\mathcal{M},\mathcal{N}})$.

We adopt a machine learning (ML) concept known as the bootstrap aggregating ensemble [34], also known as bagging ensemble, which consists of K conditional estimators, each in the form of a decision tree fitted on subsets of the covariate–target pairs using a procedure we proposed. The purpose of the ensemble, discussed in later sections, is to improve the estimate stability and statistical efficiency. The fitting process of the ensemble is illustrated in Fig. 3. The subsets are randomly sampled from the parent dataset with replacement using a procedure known as bootstrapping, where the ratio $\rho \in (0, \infty)$ controls the size of the subsets relative to their parent. Due to replacement, it is possible to create subsets larger than the original dataset. During inference, as shown in Fig. 2, the estimates $\hat{\boldsymbol{\theta}}'_{k,\mathcal{N}}(\mathbf{x}_{\mathcal{M},\mathcal{N}})$ produced by members $k = 1, \dots, K$ are averaged in the member dimension to create the final estimate $\hat{\boldsymbol{\theta}}_{\mathcal{N}}(\mathbf{x}_{\mathcal{M},\mathcal{N}})$:

$$\hat{\boldsymbol{\theta}}_{\mathcal{N}}(\mathbf{x}_{\mathcal{M},\mathcal{N}}) = \frac{1}{K} \sum_{k=1}^K \hat{\boldsymbol{\theta}}'_{k,\mathcal{N}}(\mathbf{x}_{\mathcal{M},\mathcal{N}}) \quad (8)$$

3.1. GEV parameter estimation

A well-known metric to quantify the error of probabilistic forecast $\text{Pr}_A(y; \hat{\boldsymbol{\theta}}_A)$ of distribution family A against a reference probabilistic forecast $\text{Pr}_B(y; \boldsymbol{\theta}_B)$ of distribution family B is the Kullback–Leibler divergence (KL) [35]. For observed outcome y_n , the ideal probabilistic forecast is a degenerate distribution that

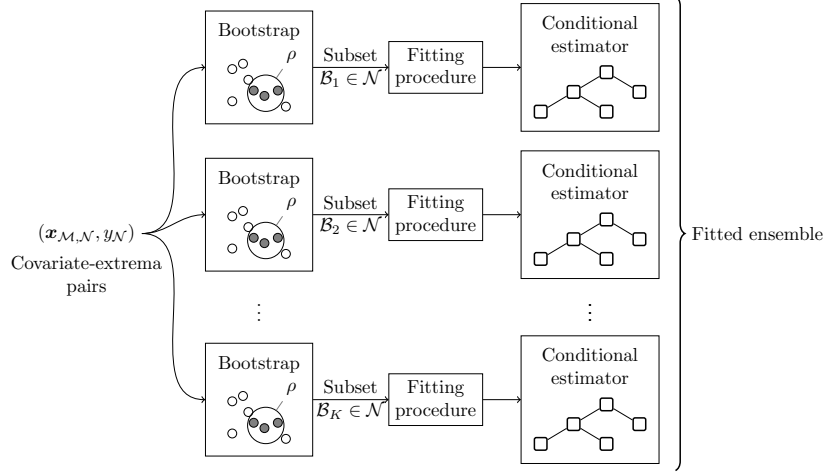


Figure 3: Ensemble fitting through bootstrapping, also known as resampling with replacement.

predicts y_n with infinite probability density denoted by the Dirac delta function $\delta(\cdot)$. As shown in eq. (9), simplification of KL against a degenerate distribution B where $\Pr_B(y; \theta_B) = \delta(y - y_n)$ leads to the log score, whose minimization results in the maximum likelihood estimate (MLE):

$$\begin{aligned}
 \text{KL}(\hat{A}, B) &= \int \Pr(y; \theta_B) \log \left(\frac{\Pr_B(y; \theta_B)}{\Pr_A(y; \hat{\theta}_A)} \right) dy \\
 &= \int \delta(y - y_n) \log \delta(y - y_n) dy - \int \delta(y - y_n) \log \Pr_A(y; \hat{\theta}_A) dy \quad (9) \\
 &= \left(\log \delta(x) \int \delta(x) dx - \int \frac{d}{dx} \log \delta(x) dx \right) - \log \Pr_A(y_n; \hat{\theta}_A) \\
 &= -\log \Pr_A(y_n; \hat{\theta}_A)
 \end{aligned}$$

The MLE for GEV does not have an explicit mathematical representation and the procedure to compute it involves an iterative process starting from an initial estimate, guided by the gradient of the log score using a method now widely known as natural gradient descent (NGD) [36]. For GEV Fisher information matrix $\mathbf{I}(\hat{\theta})$ and (ordinary) gradient ∇L of the GEV log score, the natural gradient $\tilde{\nabla} L$ is given by [37]:

$$\tilde{\nabla} L(y_n; \hat{\theta}) = \mathbf{I}^{-1}(\hat{\theta}) \cdot \nabla L(y_n; \hat{\theta}), \quad (10)$$

where τ is shown in eq. (5). For GEV, the log score is given by

$$L(y_n; \theta) = \sigma - (1 + \xi) \log \tau + \tau, \quad (11)$$

and its (ordinary) gradient is given by [38]

$$\frac{\partial L}{\partial \mu} = \frac{1}{\sigma \omega} (1 + \xi - \nu), \quad (12a)$$

$$\frac{\partial L}{\partial \sigma} = \frac{1}{\sigma} \left[-1 + \frac{1}{\sigma \omega} (1 + \xi - \nu)(y - \mu) \right], \quad (12b)$$

$$\frac{\partial L}{\partial \xi} = \frac{1}{\xi^2} \log(\omega(1 - \nu)) - \frac{1}{\sigma \omega} (1 + \xi - \nu)(y - \mu)\xi, \quad (12c)$$

$$\omega = 1 + \frac{\xi}{\sigma} (y - \mu), \quad (12d)$$

$$\nu = \omega^{-\frac{1}{\xi}}. \quad (12e)$$

For gamma function $\Gamma(x) = \int_0^\infty \tau^{x-1} \exp(-\tau) d\tau$, digamma function $\psi(x) = \partial \log \Gamma(x) / \partial x$, and Euler–Mascheroni constant $\gamma_{\text{EM}} = -\psi(1) \approx 0.5772$, Fisher information $\mathbf{I}(\boldsymbol{\theta})$ is given by [39]

$$I_{\mu\mu} = \frac{1}{\sigma^2 p}, \quad (13a)$$

$$I_{\mu\sigma} = -\frac{1}{\sigma^2 \xi} (p - \Gamma(2 + \xi)), \quad (13b)$$

$$I_{\mu\xi} = \frac{1}{\sigma \xi} \left(q - \frac{p}{\xi} \right), \quad (13c)$$

$$I_{\sigma\sigma} = \frac{1}{\sigma^2 \xi^2} (1 - 2\Gamma(2 + \xi) + p), \quad (13d)$$

$$I_{\sigma\xi} = \frac{1}{\sigma \xi^2} \left(\frac{1}{\xi} (1 - \Gamma(2 + \xi) + p) + 1 - \gamma_{\text{EM}} - q \right), \quad (13e)$$

$$I_{\xi\xi} = \frac{1}{\xi^2} \left(\frac{\pi^2}{6} + \left(1 - \gamma_{\text{EM}} + \frac{1}{\xi} \right)^2 - \frac{2q}{\xi} + \frac{p}{\xi^2} \right), \quad (13f)$$

$$p = (1 + \xi)^2 \Gamma(1 + 2\xi), \quad (13g)$$

$$q = \Gamma(2 + \xi) \left(\psi(1 + \xi) + \frac{1 + \xi}{\xi} \right). \quad (13h)$$

It has been discovered that the MLE for GEV does not exist for $\xi \leq -1$ and does not possess asymptotic consistency when $-1 < \xi \leq -0.5$ [38]. On the other hand, it is well-known that NGD on GEV is not numerically well-behaved—in addition to the need to test for singularity $\xi = 0$, where eq. (12) and eq. (13) must be replaced with their corresponding limits, due to poles in $\Gamma(x)$, $\psi(x)$, numerical evaluation of $\mathbf{I}(\hat{\boldsymbol{\theta}})$ often results in an ill-conditioned matrix that is extremely difficult to invert. As a result, checking and reconditioning of exceptional numerical cases are required to prevent divergence, resulting in computational inefficiency.

We instead adopt parameter estimation through the probability weighted moments (PWM) method [40]. Despite having a small bias, the PWM is found by [25] to have a lower bias than MLE at small sample sizes, and the advantage

can be crucial under limited data availability. In fact, due to its superior stability, PWM is often preferred over MLE in fields such as hydrology [41]. We refer the reader to [40] for a comprehensive quantitative comparison between PWM and MLE. The PWM estimate for GEV is given by

$$\hat{\xi} = -7.8590c - 2.9554c^2, \quad (14a)$$

$$\hat{\sigma} = \frac{(b_0 - 2b_1)\hat{\xi}}{\Gamma(1 - \hat{\xi})(1 - 2\hat{\xi})}, \quad (14b)$$

$$\hat{\mu} = b_0 - \frac{\hat{\sigma}}{\hat{\xi}}(\Gamma(1 - \hat{\xi}) - 1), \quad (14c)$$

and for y'_1, \dots, y'_N representing the block maxima sorted by value in ascending order, the quantities b_0, b_1, b_2, c are given by

$$b_0 = \frac{1}{N} \sum_{j=1}^N y'_j, \quad (15a)$$

$$b_1 = \frac{1}{N} \sum_{j=1}^N \frac{j-1}{N-1} y'_j, \quad (15b)$$

$$b_2 = \frac{1}{N} \sum_{j=1}^N \frac{(j-1)(j-2)}{(N-1)(N-2)} y'_j, \quad (15c)$$

$$c = \frac{2b_1 - b_0}{3b_2 - b_0} - \frac{\log 2}{\log 3}. \quad (15d)$$

3.2. Construction of the conditional estimators

We base our procedure on [42], known as classification and regression trees (CART). It is a recursive partitioning algorithm that, during fitting, dichotomizes the covariate-target pairs using a set of automatically discovered splitting rules, which are organized in the form of a tree. In the prediction phase, the splitting rules are applied to the given covariate in topological order, resulting in the activation of one of the leaf partitions whose estimate gives rise to the prediction. For set of covariate dimensions \mathcal{M} , parent observation indices \mathcal{P} and parent partition $(\mathbf{x}_{\mathcal{M},\mathcal{P}}, y_{\mathcal{P}})$, the child observation indices \mathcal{L}, \mathcal{R} resulting from splitting the parent in covariate dimension m on threshold u are:

$$\mathcal{L} = \{p|p \in \mathcal{P} \wedge \mathbf{x}_{m,p} \leq u\} \quad (16a)$$

$$\mathcal{R} = \{p|p \in \mathcal{P} \wedge \mathbf{x}_{m,p} > u\} \quad (16b)$$

The tuple (m, u) is known as the splitting rule of the partition. In CART, the selection of the optimal splitting rule is based on maximizing the reduction in squared error impurity, resulting in children in which target observations are similar in value. However, targets in the same partition do not necessarily have the same distribution. We hence modified CART, using the GEV log score eq. (11) to select the optimal splitting rule. For covariate-target pairs $(\mathbf{x}_{\mathcal{M},\mathcal{N}}, y_{\mathcal{N}})$, the procedure to construct the conditional estimators is described as follows:

- S1 The modified CART begins with the creation of a root node to which all covariate–target pairs are assigned.
- S2 A covariate dimension is selected, starting with $m = 1$. The unique values in the dimension are sorted, considering the midpoints as candidates for the splitting threshold. For each candidate splitting rule (m, u) , transient partitions y_L, y_R are created via eq. (16). The GEV PWM estimates and log scores are computed on y_L, y_R via eq. (14) and eq. (11), respectively. For parent log score L_p , and children log scores L_l, L_r , we define the impurity drop T as the reduction of the children log scores relative to the parent:

$$T = \frac{1}{L_p}(L_p - L_r - L_l) \quad (17)$$

The splitting rule that results in the maximum impurity drop is selected as the optimal rule of the partition.

- S3 The leaf nodes are scanned, and the leaf whose optimal rule results in the maximum impurity reduction is selected as the growing leaf. The optimal splitting rule of the leaf is finally applied to create the child partitions, which are inserted under the leaf. Step 2 is repeated recursively on the new children.

While CART adopts post-processing procedures known as pruning to trim certain branches to reduce the complexity of the tree, we adopt early termination, also known as pre-pruning, to suppress over-fitted branches during tree construction. The conditions for early termination are:

- The optimal threshold search in Step 2 is limited to those that result in partitions of at least a specified minimum size. A larger partition results in more accurate PWM estimates. We found that a minimum partition size of 20–50 covariate–target pairs often yields satisfactory results.
- No further children are allowed under a branch if the maximum impurity reduction of its leaf is lower than a specified limit T_{crit} . We found through experiments that T_{crit} in the range of 0.0001–0.01 often results in satisfactory results.
- The number of growing iterations is limited to a specified maximum. We found through experiments that it should be kept as large as computationally manageable, such as a value of 40.

To illustrate the fitting procedure, we extracted the runtime data from one of the conditional estimators in the bagging ensemble during fitting of the example in Section 4 and provided it in Fig. 4. The artwork illustrates the top few nodes of only one of the conditional estimators, and the bagging ensemble consists of a large number of these conditional estimators. We encourage the reader to cross-examine Fig. 4 with the procedure described in Steps 1 to 3 to understand the fitting process.

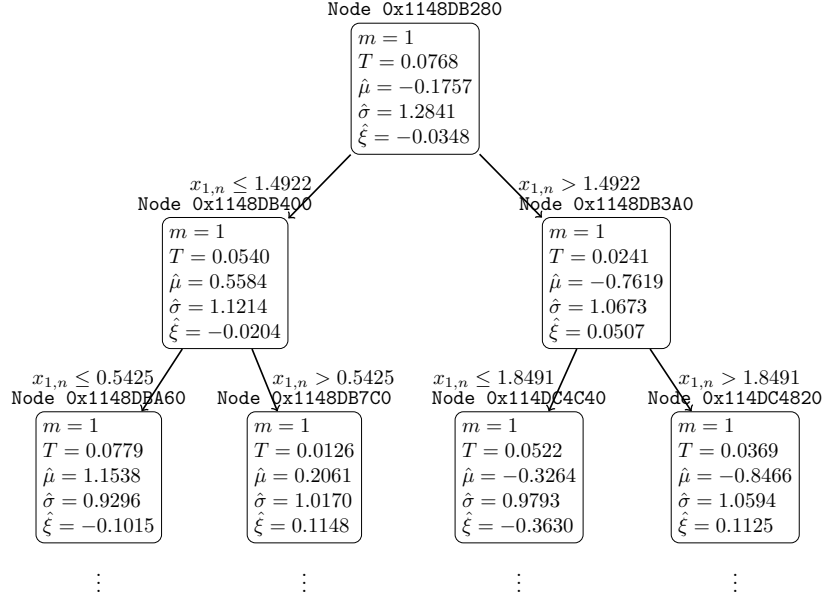


Figure 4: Structure of one of the conditional estimators created during fitting. The artwork is intended to illustrate the fitting procedure. Deeper nodes are not shown to conserve ink.

4. Application-neutral example

We envision that our approach may become broadly applicable in the scientific domain and herein present an application-neutral example to benefit a wider audience before presenting a power system-specific case study in the next section. Different from the case study, the theoretical nature of this example enables the calculation of a true reference for the quantile estimate and allows straightforward comparisons of our approach and a competitor against the known reference. The data for the example consists of $\mathcal{N} = \{1, \dots, 1000\}$ covariate–target pairs where the covariate $\mathbf{x}_{\mathcal{M}, \mathcal{N}}$ has one dimension $\mathcal{M} = \{1\}$ and the pairs are synthesized according to the following rules:

$$x_{1, \mathcal{N}} \in [0, \pi], \quad (18a)$$

$$y_{\mathcal{N}} \sim \text{GEV}(\mu_{\mathcal{N}}, \sigma_{\mathcal{N}}, \xi_{\mathcal{N}} | \mathbf{x}_{\mathcal{M}, \mathcal{N}}), \quad (18b)$$

where the instantaneous distribution parameters are given by

$$\mu_n(x_{1, n}) = \cos(1.23x_{1, n}) + 0.3 \cos(4.56x_{1, n}), \quad (19a)$$

$$\xi_n(x_{1, n}) = 0.3 \cos(5.67x_{1, n}), \quad (19b)$$

$$\sigma_n(x_{1, n}) = 1 + 0.1 \cos(6.78x_{1, n}). \quad (19c)$$

The proposed log-score-based splitting criteria are sensitive to variations in the data, and thus, the ensemble approach we adopted is crucial in improving

the quality of the estimates. Using number of ensemble members $K = 50$, minimum partition size of 20, and minimum impurity reduction $T_{\text{crit}} = 0.0001$, resample ratio $\rho = 1$, the GEV distribution estimated using our approach is visualized in the form of the 90% prediction interval against the synthesized block maxima in Fig. 5, and the parameter estimates are shown in Fig. 6.

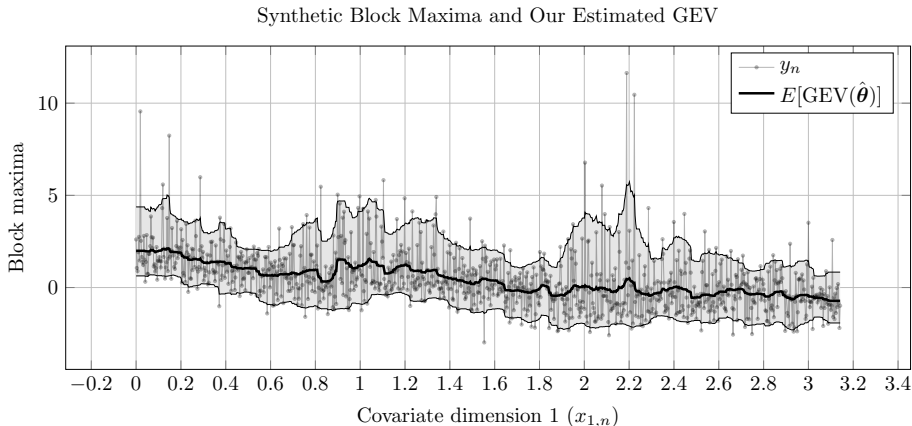


Figure 5: The synthesized block maxima and the nonstationary GEV estimated using our approach visualized in the form of its expectation and the 90% prediction interval (shaded region). GEV—generalized extreme value distribution.

A robust estimator should produce consistent estimates on samples drawn from the same distribution, despite the observations being different each time. The bias relates to the asymptotic accuracy of the estimator, and the variance relates to the stability of the estimate. The achievable minimum asymptotic variance of the estimates produced by an unbiased estimator known as the minimum-variance unbiased estimator (MVUE) is given by the Cramér-Rao bound (CRB) as follows:

$$\text{Var}(\hat{\boldsymbol{\theta}}) \geq I^{-1}(\boldsymbol{\theta}), \quad (20)$$

where $I(\boldsymbol{\theta})$ is the GEV Fisher information given by eq. (13). An unbiased estimator that achieves the CRB is considered statistically most efficient. To contrast our approach, we graphically represent the 90% parameter confidence intervals of the MVUE calculated using the diagonal elements of eq. (20) in the shaded regions of Fig. 6. Since the PWM method is biased, a test for significant parameter deviation, such as the Wald test [43], would not be well-calibrated. Nonetheless, it can be observed that our estimates fall within the interval, a graphical indication that such tests would likely be unable to reject the hypothesis that there are no statistically significant deviations between our estimates and the true parameters.

4.1. Comparison with a state-of-the-art parametric competitor

GAMLSS [20] provides a flexible framework that can approximate the parameters of a variety of distribution families as smooth functions of the covari-

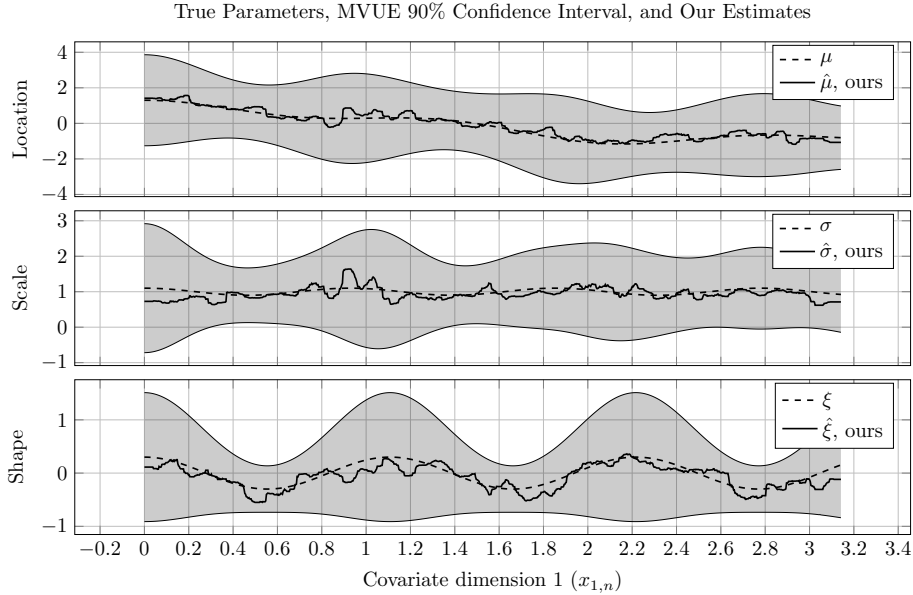


Figure 6: The true parameters of the distribution that synthesized the block maxima, the 90% confidence interval of a theoretical and ideal MVUE (shaded region), and the estimates produced by our approach. MVUE—minimum variance unbiased estimator.

ate. It is widely used in applications such as climatology [44] and public health [45] to model the variation of probability densities in response to environmental factors. However, GAMLSS comes with several notable practical drawbacks:

- GAMLSS requires the labor-intensive manual specification of formulas for all three GEV parameters through trial-and-error, which makes the forecasting model prone to misspecification.
- Spline-based function approximations are not well-suited to capturing discontinuous or highly nonlinear relationships that may be encountered during peak demand probabilistic modeling.
- GAMLSS can suffer from over-smoothing or under-fitting, where the estimates fail to adequately capture the behavior of the distribution parameters.

To empirically validate these limitations, we compared our method with GAMLSS on the same dataset described earlier. All three GEV parameters in the GAMLSS model are approximated using penalized B-splines of the covariate $\mathbf{x}_{1,n}$. The estimates of our method and those of GAMLSS are displayed in Fig. 7 against the true parameters.

For a more precise quantitative comparison, we use the continuous ranked probability score (CRPS), a robust scoring metric frequently used in forecast verification in numerical weather prediction. The CRPS compares the CDF of the

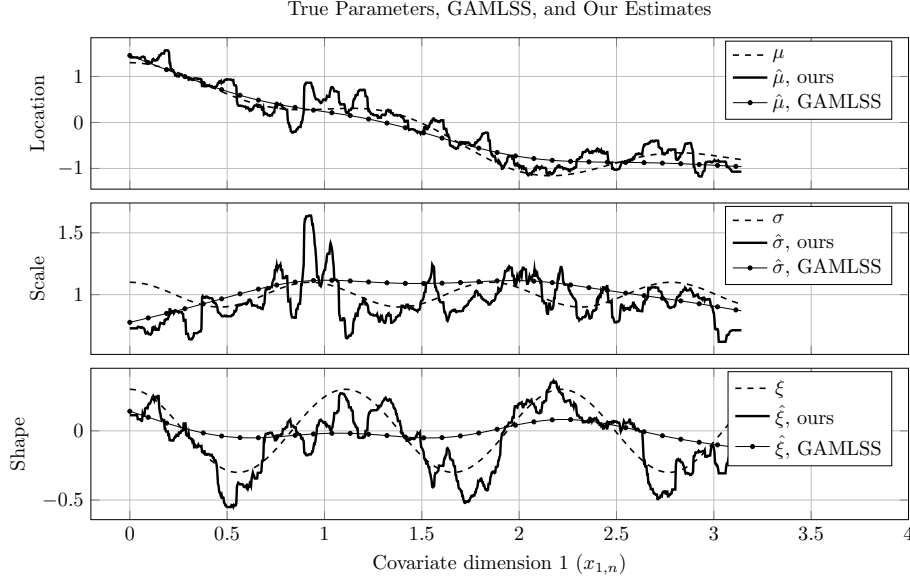


Figure 7: The true parameters of the distribution that synthesized the block maxima, the estimates produced by our approach, and the estimates produced by GAMLSS. GAMLSS—generalized additive model for location, scale, and shape.

predicted density against an ideal CDF corresponding to each observation. For gamma function $\Gamma(x) = \int_0^\infty \tau^{x-1} \exp(-\tau) d\tau$, lower incomplete gamma function $\Gamma_l(s, x) = \int_0^x t^{s-1} \exp(-t) dt$, exponential integral function $\text{Ei}(x) = \int_{-\infty}^x e^t / t dt$, and Euler–Mascheroni constant $\gamma_{\text{EM}} = -\psi(1) \approx 0.5772$, the CRPS formula for GEV is derived by [46] as follows:

$$S(y, \hat{\theta}) = \begin{cases} \left(\hat{\mu} - y - \frac{\hat{\sigma}}{\hat{\xi}} \right) (1 - 2F_{\xi \neq 0}(y)) & \hat{\xi} \neq 0, \\ -\frac{\hat{\sigma}}{\hat{\xi}} \left(2\hat{\xi}\Gamma(1 - \hat{\xi}) - 2\Gamma_l(1 - \hat{\xi}, -\log F_{\xi \neq 0}(y)) \right), & \hat{\xi} \neq 0, \\ \hat{\mu} - y + \hat{\sigma}(\gamma_{\text{EM}} - \log 2) - 2\hat{\sigma}\text{Ei}(\log F_{\xi=0}(y)), & \hat{\xi} = 0, \end{cases} \quad (21)$$

where $F(y)$ is the CDF of GEV, given by

$$F(y) = \exp(-\tau), \quad (22)$$

and τ is shown in eq. (5). The CRPS of our method and GAMLSS on the previously described dataset is listed in Table 2. The scores shown are the average CRPS over all observations, and the per-observation CRPS is calculated via eq. (21). A lower score indicates better agreement between the observations and the CDF of the estimated density.

GAMLSS CRPS	Our CRPS
0.719	0.677

Table 2: Comparison of the CRPS between our approach and GAMLSS in the application-neutral example. CRPS—continuous ranked probability score, GAMLSS—generalized additive model for location, scale, and shape.

4.2. Exploring the limitation of a quantile-based non-parametric competitor

In terms of nonparametric competitors, since the block maxima in the example follow a nonlinear relationship with the covariate $\mathbf{x}_{\mathcal{M},\mathcal{N}}$, linear approaches such as QR would discernibly be out-competed by our approach, which can model nonlinear relationships. To present a fair case-by-case comparison across different quantiles, we computed the block maxima quantile estimates from our results using the inverse CDF shown in eq. (23) and compared them with the true quantile targets based on eq. (19) and quantile estimates of quantile regression forest (QRF) [47]. The results are shown in Fig. 8 and Fig. 9.

$$F^{-1}(\alpha; \boldsymbol{\theta}) = \begin{cases} \mu - \sigma \log(-\log \alpha) & \xi = 0, \\ \mu + \frac{\sigma}{\xi} ((-\log \alpha)^{-\xi} - 1) & \xi \neq 0. \end{cases} \quad (23)$$

It can be observed in Fig. 8 that our approach outperforms QRF in all evaluated quantiles and especially at the LPHC quantiles. In Fig. 9, for quantiles 0.1, 0.5, and 0.9, the estimates of QRF are especially noisy compared to our estimates and the true block maxima targets, suggesting some level of over-fitting by QRF. Given that an over-fitted QRF possesses increased sensitivity to extreme observations, for LPHC quantiles 0.999 and 0.999999, however, the QRF estimates deviate significantly from the true targets, while the quantile estimates produced by our approach are in significantly better agreement with the true targets. The scarcity of extreme observations limits the ability of quantile-based methods, including highly sophisticated deep-learning-based quantile regression methods, to accurately approximate distribution tails. Quantile methods are often out-competed in terms of accuracy and trustworthiness by EVA in critical applications such as finance and insurance underwriting. For more comprehensive comparisons between quantile-based methods and EVA, we refer the reader to [48, 49, 50].

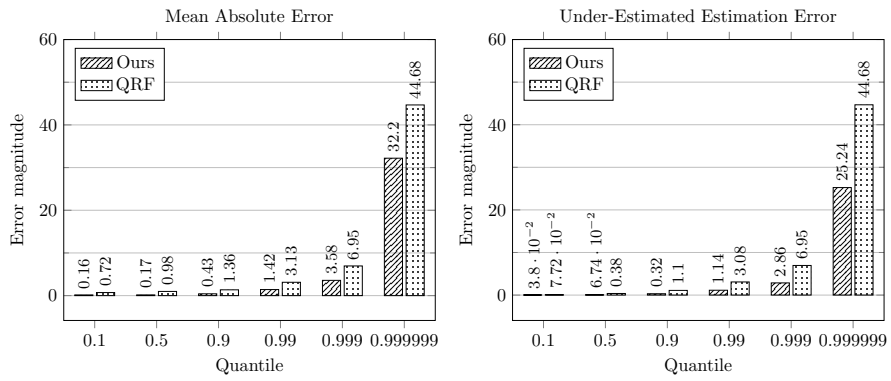


Figure 8: The errors between quantile estimates given by QRF and our approach against the true quantile target of the distribution that synthesized the block maxima. QRF—quantile regression forest.

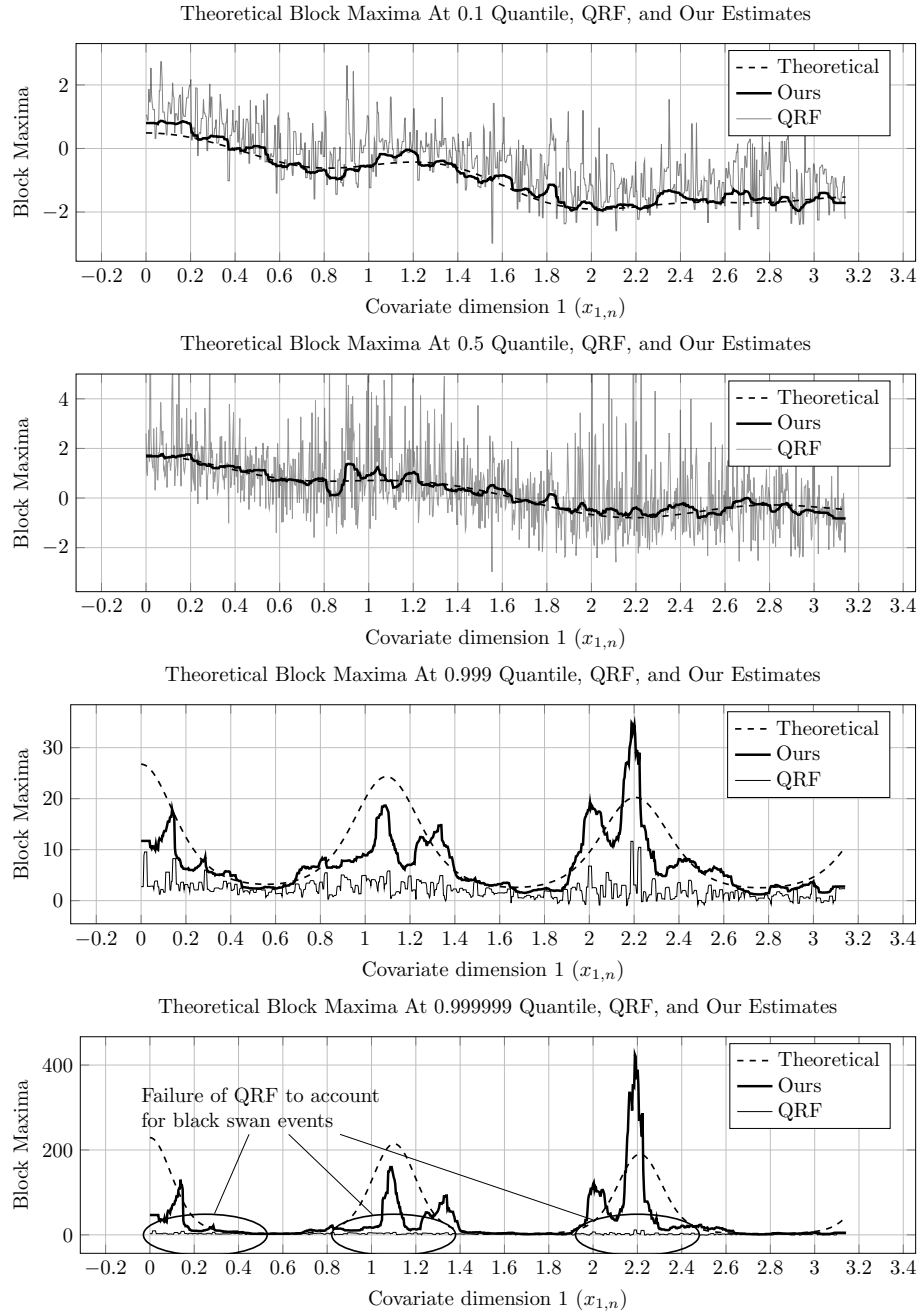


Figure 9: The quantile estimates given by QRF and our approach and the true quantile target of the distribution that synthesized the block maxima. Note that the vertical axis differs in scale considerably between plots. QRF—quantile regression forest.

5. Case study—day-ahead scheduling capacity determination

The PJM interconnection is a regional transmission organization (RTO) serving 65 million people across 13 states and the District of Columbia. The system demand ranges between 80 GW to 150 GW, the summer peak in 2024 exceeding 152 GW. The simplified block diagram of the scheduling workflow of PJM is shown in Fig. 10.

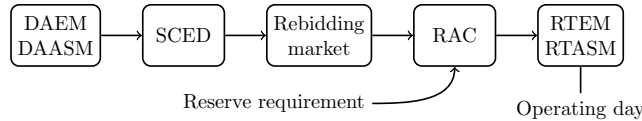


Figure 10: Simplified block diagram of the scheduling workflow of PJM. DAEM—day-ahead energy market, DAASM—day-ahead ancillary service market, SCED—security-constrained economic dispatch, RAC—reliability assessment and commitment, RTEM—real-time energy market, RTASM—real-time ancillary service market.

According to PJM Manual 11 [51], offers and bids are submitted into the day-ahead markets by market participants. Following the closure of the markets at 11:00 ahead of the operating day, PJM performs market clearing through the security-constrained economic dispatch (SCED) engine to select the most economic generation offers while ensuring generation is sufficient to satisfy demand. The hourly generation schedule, locational marginal price (LMP), and market clearing price (MCP) determined by SCED are posted before 13:30, and winners are allowed to make adjustments to the cleared schedules through the rebidding market, which closes at 14:45. PJM then performs a second resource commitment known as the reliability assessment and commitment (RAC), which ensures sufficient generation capacity is scheduled to meet the reserve requirements for the next operating day as the activities progress to the real-time markets at midnight.

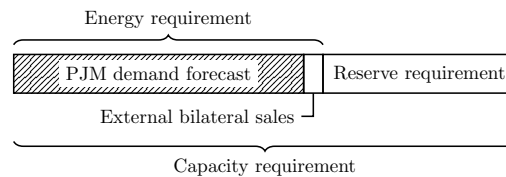


Figure 11: Composition of the day-ahead scheduling capacity.

To prepare for possible contingencies and maintain energy balance under operational uncertainty, additional generation resources known as reserves are scheduled by RAC based on Fig. 11 and placed on standby during the operating day. In this case study, we apply our approach and demonstrate a risk-based day-ahead scheduling capacity (DASC) requirement determination method. For simplicity, the case study only considers total system demand within the PJM RTO region. External bilateral sales and scheduled interchanges with neighboring balancing authority areas are ignored.

5.1. Data origin and fitting

The PJM Data Miner 2 platform [52] provides a variety of publicly-accessible datasets. We obtained the demand hourly integrated average (HIA), hourly demand forecasts, and historical day-ahead temperature forecasts for study years 2022–2024 from the platform. The PJM demand forecasts are updated every 6 hours and predict the demand for each hour of an entire day in the form of single-valued point estimates. The forecasts are highly accurate and according to PJM Manual 11 [51], are obtained using a combination of neural net and pattern-matching approaches. Based on our recommendation in Subsection 2.2, we create daily peak probabilistic predictions based on the PJM point prediction and delegate the responsibility of modeling autocorrelation to the PJM forecast—we assume the daily peak follows the conditional distribution $y \sim \text{GEV}(\boldsymbol{\theta}|\mathbf{x})$ whose covariate \mathbf{x} is shown in Fig. 12. To integrate our approach into the PJM workflow in Fig. 10, the capacity requirements need to be available at least 36 hours in advance for the RAC run at 14:45, leading us to adopt the demand forecasts produced at 05:45 ahead of the operating day.

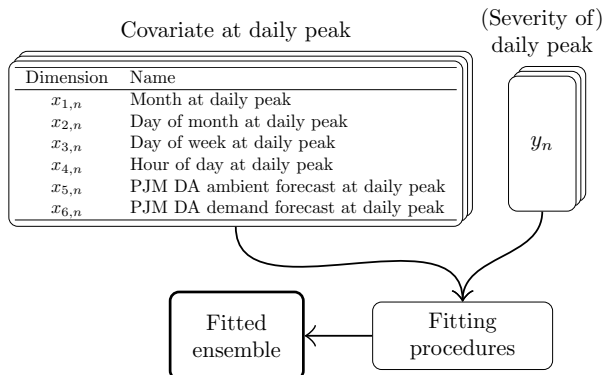


Figure 12: The fitting data contains only the daily peaks and the corresponding covariate, whose structure is shown in the figure. DA—day-ahead.

The forecasting ensemble is fitted to the covariate-peak pairs $(\mathbf{x}_{\mathcal{M},\mathcal{N}}, y_{\mathcal{N}})$ in study years 2022–2023 using number of ensemble members $K = 50$, resampling ratio $\rho = 1$, the minimum impurity drop $T_{\text{crit}} = 0.05$, and the minimum number of covariate-target pairs of each partition limited to no less than 30. Data for test year 2024 is held confidential to the fitting procedures. We define the residual $r_{\mathcal{N}}$ as the difference between the statistical expectation of the predicted peak distribution and the actual daily peak $y_{\mathcal{N}}$:

$$r_{\mathcal{N}} \triangleq \hat{y}_{\mathcal{N}} - y_{\mathcal{N}} = \mathbb{E} \left[\text{GEV}(\hat{\boldsymbol{\theta}}|\mathbf{x}_{\mathcal{M},\mathcal{N}}) \right] - y_{\mathcal{N}}, \quad (24)$$

and the expectation is given by

$$\mathbb{E} [\text{GEV}(\boldsymbol{\theta})] = \begin{cases} \mu + \frac{\sigma}{\xi} (\Gamma(1 - \xi) - 1) & \xi \in (-\infty, 1) \setminus \{0\}, \\ \mu + \sigma\gamma_{EM} & \xi = 0, \\ \infty & \xi \geq 1. \end{cases} \quad (25)$$

The residuals of a robust forecasting algorithm should follow a stationary normal distribution with a small mean and variance. It can be observed from Fig. 13 that the residuals in study years 2022–2023 appear to follow a normal distribution. Following fitting, covariates of test year 2024 are supplied to the ensemble, resulting in forecasts for the entire study year in the form of GEV parameter estimates for the daily peak that are updated hourly as conditions change. As a consequence of including the highly accurate PJM point forecast in the covariate, the mean absolute error (MAE) of the forecasted daily peak expectation against the actual daily peaks in test year 2024 is 2814.28 MW, or 1.84% of the 153 GW total system demand. The mean under-forecasted forecasting error of the daily peak is 1850.15 MW, or 1.21% of the total system demand.

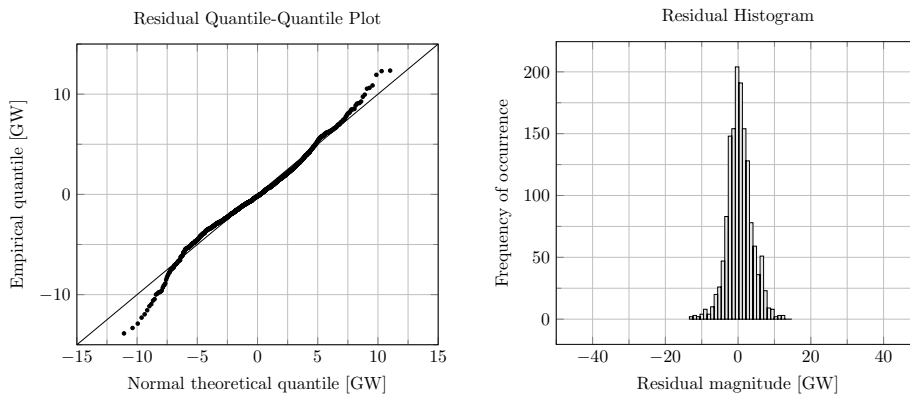


Figure 13: Quantile-quantile plot and histogram of the daily peak residuals in study years 2022–2023.

5.2. Results: day-ahead scheduling capacity

According to PJM Manual 13 [53], the DASC 30-minute reserve requirement is calculated based on the annual peak load forecast adjusted for the under-forecasted load-forecasting error and generator forced outage rate (FOR). On the other hand, the determination of required reserves in long- and near-term planning follows the “one day in ten years” guideline specified by NERC standard BAL-502-RF-03 [9] based on the LOLP, defined as the probability of demand exceeding the available generation capacity. The NERC guideline requires the annual LOLP to be equal to 0.1 and generalizes into daily LOLP risk

requirement η as follows:

$$\eta = \frac{0.1 \text{ Events/year}}{365 \text{ days/year}} = 273.9 \times 10^{-6} \text{ Events/d} \quad (26)$$

It can be argued that it is possible for the PJM method to over-commit the DASC over low-risk periods of the year, resulting in unnecessary increases in wholesale energy prices. Numerous papers propose alternatives and demonstrate risk-averse stochastic scheduling methods, such as [54, 55] on microgrids, and [56] on renewable energy systems. The required generation capacity to control the LOLP to risk level η corresponds to an extreme quantile and as demonstrated in Section 4, is difficult to accurately estimate using non-EVA approaches. Therefore, we critique the aforementioned papers for the lack of a comprehensive statistical framework to accurately model extreme values and critical system risks.

For the event \mathcal{Y} that the daily peak occurs at hourly condition \mathbf{x} , joint probability $\Pr(y, \mathcal{Y}|\mathbf{x}_n)$ of daily peak of severity y occurring under hourly condition \mathbf{x}_n , the DASC that can accommodate the daily peak under risk level η satisfies

$$\begin{aligned} \Pr(y > \text{DASC}_n, \mathcal{Y}|\mathbf{x}_n) &\leq \eta, \\ \Rightarrow \Pr(y > \text{DASC}_n; \hat{\boldsymbol{\theta}}_n|\mathbf{x}_n) \Pr(\mathcal{Y}|\mathbf{x}_n) &\leq \eta, \end{aligned} \quad (27)$$

where the conditional daily peak density $\Pr(y; \hat{\boldsymbol{\theta}}_n|\mathbf{x}_n)$ is estimated using our approach. As discussed in Section 2, under worst-case baseline probability $\Pr(\mathcal{Y}|\mathbf{x}_n) \equiv 1$,

$$\begin{aligned} \Pr(y > \text{DASC}_n; \hat{\boldsymbol{\theta}}_n|\mathbf{x}_n) &\leq \eta, \\ \Rightarrow \text{DASC}_n &\geq F^{-1}(\alpha; \hat{\boldsymbol{\theta}}_n) = \text{VaR}_n(\alpha), \end{aligned} \quad (28)$$

where confidence $\alpha = 1 - \eta$ and $F^{-1}(\alpha; \boldsymbol{\theta}_n)$, also known as the value-at-risk (VaR), is calculated via eq. (23). The relationship between the VaR, the inverse CDF, the DASC, and the LOLP is displayed in Fig. 14.

The DASC determined from the daily risk requirement η changes each hour as conditions change and is displayed in Fig. 15, contrasted by the actual demand HIA and the PJM DASC determined from the economic maximum of generating offers cleared in the day-ahead energy market (DAEM). Over the two high-risk months shown in Fig. 15, our DASC enveloped the demand curve and it can be observed that around the 133 GW winter peak on January 17 and around the 152 GW summer peak on July 16, compared to previous and subsequent days, our approach increased the capacity to compensate for the increased risk, while the PJM DASC stayed largely unchanged, indicating a potential for over-commitment. The sum of the committed hourly capacity of PJM in study year 2024 is 1 470 573 GWh, while that of approach is 910 052 GWh, a 38% reduction. It can be concluded that adopting our approach would result in significant cost savings by committing capacity only as much as needed to maintain the risk requirement.

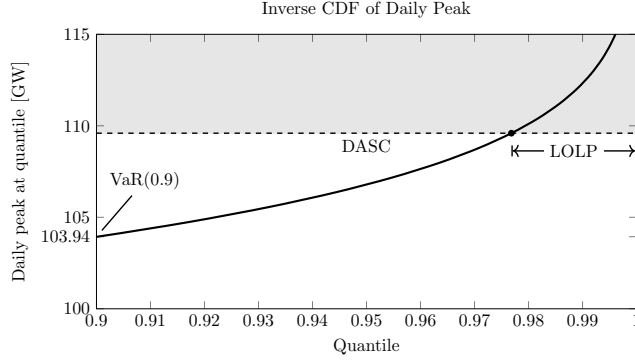


Figure 14: Relationship between the inverse CDF, the VaR, the DASC, and the LOLP. CDF—cumulative distribution function, VaR—value-at-risk, DASC—day-ahead scheduling capacity, LOLP—loss-of-load probability.

5.3. Results: expected unserved energy

The EUE is defined as the expected total amount of unserved energy in a time horizon due to capacity shortage. It is typically presented in megawatt hours and used as an annual risk indicator. Using our approach, however, we can estimate the EUE in daily resolution. In a maximum capacity emergency, the day-ahead EUE can help the RTO identify the most likely amount and duration of load shedding during the operating day to restore energy balance, whether energy conservation directives and DSM alone would suffice, and whether critical loads would be affected. Assuming worst-case baseline probability $\Pr(\mathcal{Y}|\mathbf{x}_n) \equiv 1$ where condition \mathbf{x}_n of hour n always results in the daily peak, the daily EUE under the DASC determined from eq. (28) based on confidence $\alpha = 1 - \eta$ is given by

$$\begin{aligned}
 \text{EUE} &= \sum_{n=1}^{24} \left(\int_{\text{VaR}_n(\alpha)}^{\infty} (y - \text{VaR}_n(\alpha)) \Pr(y|\mathcal{Y}, \mathbf{x}_n) \Pr(\mathcal{Y}|\mathbf{x}_n) dy \right) \\
 &= \sum_{n=1}^{24} \int_{\text{VaR}_n(\alpha)}^{\infty} dy \left(y \Pr(y; \hat{\theta}|\mathbf{x}_n) - \text{VaR}_n(\alpha) \Pr(y; \hat{\theta}|\mathbf{x}_n) \right) \quad (29) \\
 &= (1 - \alpha) \sum_{n=1}^{24} (\text{CVaR}_n(\alpha) - \text{VaR}_n(\alpha)),
 \end{aligned}$$

and for lower incomplete gamma function $\Gamma_l(s, x) = \int_0^x t^{s-1} \exp(-t) dt$, logarithmic integral function $\text{li}(x) = \int_0^x dx / \log x$, the conditional value-at-risk (CVaR) is given by

$$\text{CVaR}(\alpha) = \begin{cases} \mu + \frac{\sigma}{1-\alpha} [\gamma_{\text{EM}} - \text{li}(\alpha) + \alpha \log(-\log \alpha)] & \xi = 0, \\ \mu + \frac{\sigma}{(1-\alpha)\xi} [\Gamma_l(1 - \xi, -\log \alpha) - (1 - \alpha)] & \xi \neq 0. \end{cases} \quad (30)$$

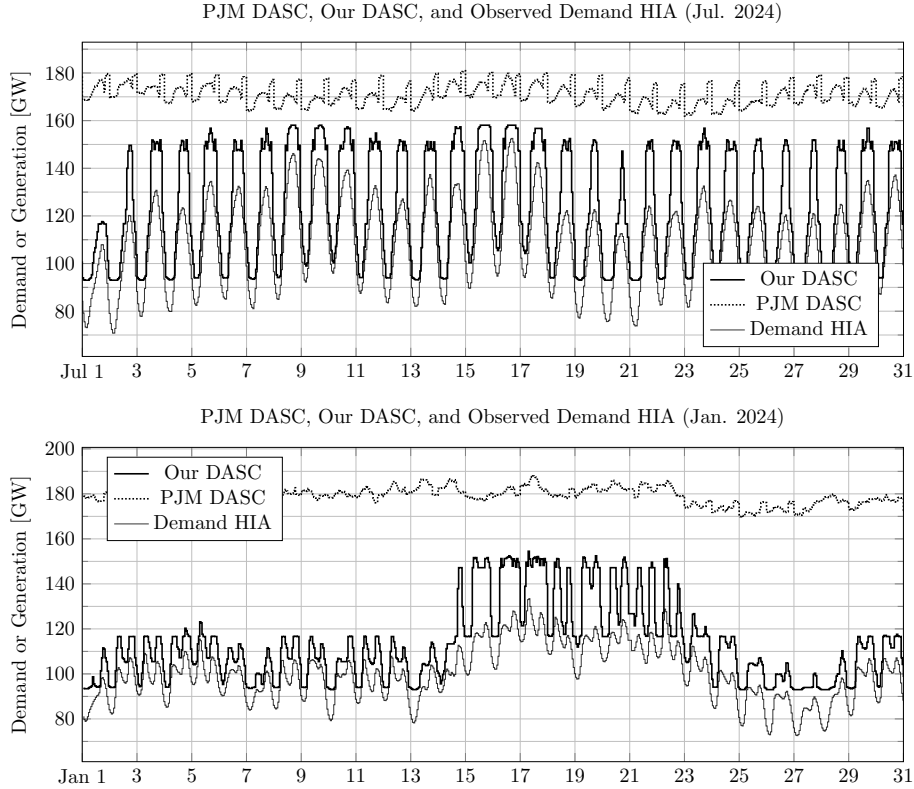


Figure 15: Comparison between the DASC determined from our approach, the DASC determined by PJM, and the demand HIA in high-risk months of study year 2024. DASC—day-ahead scheduling capacity, HIA—hourly integrated average.

The EUE determined from eq. (29) for study year 2024 is shown in Fig. 16. It can be observed that in terms of magnitude, severe EUE occurs in the winter, while in terms of surface area, however, the EUE accumulates in the summer. We calculated the annual sum of the daily EUE to compare with annual EUE metrics from the industry. Assuming the adoption of our approach for the DASC via the LOLP guideline in eq. (26), the estimated annual EUE in study year 2024 is 32.37 MWh, or 0.04 PPM (parts per million) of the 799 269.28 GWh total demand. The EUE of PJM is not publicly disclosed. However, an industry presentation reported a normalized EUE of 1 PPM [26] for a different RTO.

5.4. Results: exploring a state-of-the-art competitor

We attempted to apply the previously described competitor framework GAMLSS¹ to the case study using the same covariate structure shown in 12. The location,

¹gamlss R package, version 5.4-22

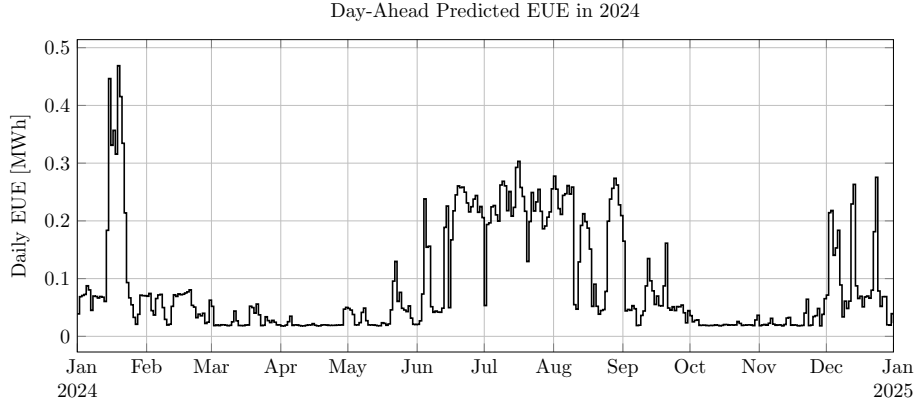


Figure 16: Predicted daily EUE in study year 2024. EUE—expected unserved energy.

scale, and shape parameters of the GEV are modeled as penalized B-splines of the PJM day-ahead demand forecast and PJM day-ahead ambient temperature. Day of week, day of month, and month are treated as categorical variables. Despite attempting different covariate element combinations, the competitor GAMLSS failed to converge in all tested configurations. This reinforces the limitation of GAMLSS in irregular data settings described in previous sections and is consistent with the findings of [21]. Consequently, GAMLSS is excluded from comparison in this case study. We refer the reader to Section 4 where GAMLSS successfully converged for comparison of GAMLSS with our approach.

6. Conclusion

Risk-sensitive power system planning and scheduling require accurately characterizing the probability and severity of the peak demand. To overcome the stationarity limitation of classical EVA, energy regulatory and oversight agencies combine EVA with Monté-Carlo simulations for annual peak assessments, but per-scenario simulations become intractable at higher time resolutions, such as day-ahead scheduling. Whereas literature favors assumption-free quantile forecasting methods that can model nonstationarity, we demonstrated through an example that such non-EVA approaches fail to estimate critical “black swan” events due to the rarity of observations at extreme quantiles. In our case study, we reinforced findings in the literature that the state-of-the-art alternative GAMLSS can suffer from convergence issues in high-dimensional covariate cases. To adopt EVA in higher time resolutions, an innovative nonstationary estimator must be developed.

Leveraging established ML techniques and EVA, we devised a rigorous conditional statistical framework to model nonstationary extrema densities, clearly presented the assumptions, and addressed the weakening of the framework due to autocorrelation. Based on the framework, we developed and elaborated on a

novel nonstationary EVA parameter estimation approach, contrasted it with a theoretically most efficient estimator, state-of-the-art GAMLSS, and a quantile-based competitor through an experiment, and presented its real-world application through a case study. As we discovered from the case study, the capacity determination method in the industry lacks resolution and cannot distinguish high and low-risk periods of the year, resulting in over-commitment of resources. Our approach only schedules as much capacity as needed to maintain the given risk requirement, achieving a 38% reduction in yearly total committed capacity, resulting in potentially significant savings in wholesale electricity prices. This paper opens the door to numerous research directions utilizing nonstationary EVA within and beyond power systems engineering.

Acknowledgements

- This paper is partly derived from the work supported by the U.S. Department of Energy’s Office of Energy Efficiency and Renewable Energy (EERE) through the Solar Energy Technology Office (SETO) under Award DE-EE0009357. We thank the agency for its financial support. The funding source has no involvement in the development of the methodology, design, preparation, or interpretation of the case study, or the decision to submit for publication.
- We would like to thank Haley Northrup for her support in improving this paper’s organization, wording, clarity, and impact-related aspects.

Declaration of generative AI and AI-assisted technologies in the writing process

During the preparation of this work, the authors utilized generative artificial intelligence (AI) tools that include ChatGPT, ScholarGPT, and Consensus to assist in the discovery of relevant publications in academia and from the industry, and NotebookLM in the indexing and categorization of acquired public-domain training materials, presentations, manuals, and white papers obtained from PJM, ISO New England, and NERC. Although some statements are informed by AI-generated text, the paper does not contain AI-generated content, and information provided by AI has been critically examined, thoroughly substantiated, and rigorously vetted by the authors. The authors take full responsibility for the content of the published article.

References

- [1] N. M. Flores, H. McBrien, V. Do, M. V. Kiang, J. Schlegelmilch, J. A. Casey, The 2021 Texas Power Crisis: distribution, duration, and disparities, *Journal of Exposure Science & Environmental Epidemiology* 33 (1) (2023) 21–31. doi:10.1038/s41370-022-00462-5.

- [2] NERC, Probabilistic Assessment, Technical Guideline Document, North American Electric Reliability Cooperation (Aug. 2016).
URL https://www.nerc.com/comm/RSTC/PAWG/proba_technical_guideline_document_08082014.pdf
- [3] S. George, J. Zhao, Preliminary Results of Energy Adequacy Studies for Winter 2027 (May 2023).
URL https://www.iso-ne.com/static-assets/documents/2023/05/a10_operational_impact_of_extreme_weather_events.pdf
- [4] T. S. Dillon, K. W. Edwin, H.-D. Kochs, R. J. Taud, Integer Programming Approach to the Problem of Optimal Unit Commitment with Probabilistic Reserve Determination, *IEEE Transactions on Power Apparatus and Systems* PAS-97 (6) (1978) 2154–2166. doi:10.1109/TPAS.1978.354719.
- [5] L. Shi, J. Hao, J. Zhou, G. Xu, Ant colony optimization algorithm with random perturbation behavior to the problem of optimal unit commitment with probabilistic spinning reserve determination, *Electric Power Systems Research* 69 (2) (2004) 295–303. doi:10.1016/j.epsr.2003.10.008.
- [6] S. E. Haupt, M. Garcia Casado, M. Davidson, J. Dobschinski, P. Du, M. Lange, T. Miller, C. Mohrlen, A. Motley, R. Pestana, J. Zack, The Use of Probabilistic Forecasts: Applying Them in Theory and Practice, *IEEE Power and Energy Magazine* 17 (6) (2019) 46–57. doi:10.1109/MPE.2019.2932639.
- [7] S. Impram, S. Varbak Nese, B. Oral, Challenges of renewable energy penetration on power system flexibility: A survey, *Energy Strategy Reviews* 31 (2020) 100539. doi:10.1016/j.esr.2020.100539.
- [8] C. Sweeney, R. J. Bessa, J. Browell, P. Pinson, The future of forecasting for renewable energy, *WIREs Energy and Environment* 9 (2) (2020) e365. doi:10.1002/wene.365.
- [9] North American Electric Reliability Corporation, BAL-502-RF-03: Planning Resource Adequacy Analysis, Assessment and Documentation (Oct. 2017).
- [10] Daniel Cornelis van Holst Pellekaan, Draft National Electricity Amendment (Interim Reliability Measure) Rule 2020.
URL https://web.archive.org/au/awa/20200921005256mp_/http://www.coagenergycouncil.gov.au/sites/prod.energycouncil/files/publications/documents/ESB%20Consultation%20-%20Draft%20National%20Electricity%20Amendment%20%28Interim%20Reliability%20Measure%29%20Rule%202020.pdf
- [11] Regulation (EU) 2019/941 of the European Parliament and of the Council of 5 June 2019 on risk-preparedness in the electricity sector and repealing Directive 2005/89/EC (Jun. 2019).

- [12] R. Koenker, G. Bassett, Regression Quantiles, *Econometrica* 46 (1) (1978) 33–50. doi:10.2307/1913643.
- [13] W. P. Jiotsop-Foze, A. Hernández-del Valle, F. Venegas-Martínez, Electrical load forecasting to plan the increase in renewable energy sources and electricity demand: a CNN-QR-RTCF and deep learning approach, Vol. 14, 2024, pp. 186–194. doi:10.32479/ijeep.15773.
- [14] H. Guo, B. Huang, J. Wang, Probabilistic load forecasting for integrated energy systems using attentive quantile regression temporal convolutional network, *Advances in Applied Energy* 14 (2024) 100165. doi:10.1016/j.adapen.2024.100165.
- [15] G. Li, R. Zhang, S. Bu, J. Zhang, J. Gao, Probabilistic prediction-based multi-objective optimization approach for multi-energy virtual power plant, *International Journal of Electrical Power & Energy Systems* 161 (2024) 110200. doi:10.1016/j.ijepes.2024.110200.
- [16] E. Waldmann, Quantile regression: A short story on how and why, *Statistical Modelling* 18 (3-4) (2018) 203–218. doi:10.1177/1471082X18759142.
- [17] M. Rosenblatt, Remarks on Some Nonparametric Estimates of a Density Function, *The Annals of Mathematical Statistics* 27 (3) (1956) 832–837. doi:10.1214/aoms/1177728190.
- [18] R. F. Engle, Autoregressive Conditional Heteroscedasticity with Estimates of the Variance of United Kingdom Inflation, *Econometrica* 50 (4) (1982) 987. doi:10.2307/1912773.
URL <https://www.jstor.org/stable/1912773?origin=crossref>
- [19] T. Bollerslev, Generalized autoregressive conditional heteroskedasticity, *Journal of Econometrics* 31 (3) (1986) 307–327. doi:10.1016/0304-4076(86)90063-1.
URL <https://linkinghub.elsevier.com/retrieve/pii/0304407686900631>
- [20] R. A. Rigby, D. M. Stasinopoulos, Generalized Additive Models for Location, Scale and Shape, *Journal of the Royal Statistical Society Series C: Applied Statistics* 54 (3) (2005) 507–554. doi:10.1111/j.1467-9876.2005.00510.x.
URL <https://academic.oup.com/jrsssc/article/54/3/507/7113027>
- [21] A. Mayr, N. Fenske, B. Hofner, T. Kneib, M. Schmid, GAMLSS for high-dimensional data - a flexible approach based on boosting (2010). doi:10.5282/UBM/EPUB.11938.
URL <https://epub.ub.uni-muenchen.de/id/eprint/11938>
- [22] N. Bousquet, *Extreme Value Theory with Applications to Natural Hazards: From Statistical Theory to Industrial Practice*, Springer International Publishing AG, Cham, 2021.

- [23] B. Renard, M. Lang, Use of a Gaussian copula for multivariate extreme value analysis: Some case studies in hydrology, *Advances in Water Resources* 30 (4) (2007) 897–912. doi:10.1016/j.advwatres.2006.08.001. URL <https://linkinghub.elsevier.com/retrieve/pii/S0309170806001461>
- [24] R. W. Katz, M. B. Parlange, P. Naveau, Statistics of extremes in hydrology, *Advances in Water Resources* 25 (8-12) (2002) 1287–1304. doi:10.1016/S0309-1708(02)00056-8. URL <https://linkinghub.elsevier.com/retrieve/pii/S0309170802000568>
- [25] E. S. Martins, J. R. Stedinger, Generalized maximum-likelihood generalized extreme-value quantile estimators for hydrologic data, *Water Resources Research* 36 (3) (2000) 737–744. doi:10.1029/1999WR900330. URL <https://agupubs.onlinelibrary.wiley.com/doi/10.1029/1999WR900330>
- [26] Z. Ming, The Role of Metrics in Determining a Reliability Standard (Sep. 2024). URL <https://cdn.misoenergy.org/20240926%20RA%20Risk%20Metric%20Workshop%20Item%2004%20Ming%20E3%20MISO%20Role%20of%20Metrics%20in%20Reliability650106.pdf>
- [27] S. Hochreiter, J. Schmidhuber, Long Short-Term Memory, *Neural Computation* 9 (8) (1997) 1735–1780. doi:10.1162/neco.1997.9.8.1735. URL <https://direct.mit.edu/neco/article/9/8/1735-1780/6109>
- [28] S. Bai, J. Z. Kolter, V. Koltun, An Empirical Evaluation of Generic Convolutional and Recurrent Networks for Sequence Modeling, arXiv:1803.01271 (Apr. 2018). doi:10.48550/arXiv.1803.01271. URL <http://arxiv.org/abs/1803.01271>
- [29] E. Castillo, *Extreme value theory in engineering, Statistical modeling and decision science*, Academic Press, Boston, 1988.
- [30] S. N. Majumdar, A. Pal, G. Schehr, Extreme value statistics of correlated random variables: a pedagogical review (2019). doi:10.48550/ARXIV.1910.10667.
- [31] M. R. Leadbetter, *Extremes and Related Properties of Random Sequences and Processes*, 1st Edition, Springer Series in Statistics Ser, Springer New York, New York, NY, 1983.
- [32] D. Ganger, J. Zhang, V. Vittal, Statistical Characterization of Wind Power Ramps Via Extreme Value Analysis, *IEEE Transactions on Power Systems* 29 (6) (2014) 3118–3119. doi:10.1109/TPWRS.2014.2315491.

- [33] Z. Wang, Z. Liu, Y. Sun, W. Gao, C. Gu, High Impact Low Frequency Peak Load Analysis using Extreme Value Theory, in: 2018 2nd IEEE Conference on Energy Internet and Energy System Integration (EI2), IEEE, Beijing, 2018, pp. 1–6. doi:10.1109/EI2.2018.8582202.
- [34] L. Breiman, Bagging predictors, *Machine Learning* 24 (2) (1996) 123–140. doi:10.1007/BF00058655.
- [35] S. Kullback, R. A. Leibler, On Information and Sufficiency, *The Annals of Mathematical Statistics* 22 (1) (1951) 79–86. doi:10.1214/aoms/1177729694.
- [36] S.-i. Amari, Natural Gradient Works Efficiently in Learning, *Neural Computation* 10 (2) (1998) 251–276. doi:10.1162/089976698300017746.
- [37] T. Duan, A. Avati, D. Y. Ding, K. K. Thai, S. Basu, A. Y. Ng, A. Schuler, NGBoost: Natural Gradient Boosting for Probabilistic Prediction (Jun. 2020). doi:10.48550/arXiv.1910.03225.
- [38] D. K. Dey, J. Yan (Eds.), *Extreme Value Modeling and Risk Analysis: Methods and Applications*, Chapman and Hall/CRC, New York, 2016. doi:10.1201/b19721.
- [39] P. Prescott, A. T. Walden, Maximum likelihood estimation of the parameters of the generalized extreme-value distribution, *Biometrika* 67 (3) (1980) 723–724. doi:10.1093/biomet/67.3.723.
- [40] J. R. M. Hosking, J. R. Wallis, E. F. Wood, Estimation of the Generalized Extreme-Value Distribution by the Method of Probability-Weighted Moments, *Technometrics* 27 (3) (1985) 251–261. doi:10.2307/1269706.
- [41] S. Coles, *An Introduction to Statistical Modeling of Extreme Values*, Springer Series in Statistics, Springer London, London, 2001. doi:10.1007/978-1-4471-3675-0. URL <http://link.springer.com/10.1007/978-1-4471-3675-0>
- [42] L. Breiman, J. Friedman, R. A. Olshen, C. J. Stone, *Classification and Regression Trees*, Chapman and Hall/CRC, New York, 2017. doi:10.1201/9781315139470.
- [43] A. Wald, Tests of Statistical Hypotheses Concerning Several Parameters When the Number of Observations is Large, *Transactions of the American Mathematical Society* 54 (3) (1943) 426–482. doi:10.2307/1990256.
- [44] M. Dabernig, G. J. Mayr, J. W. Messner, A. Zeileis, Simultaneous Ensemble Postprocessing for Multiple Lead Times with Standardized Anomalies, *Monthly Weather Review* 145 (7) (2017) 2523–2531. doi:10.1175/MWR-D-16-0413.1. URL <https://journals.ametsoc.org/doi/10.1175/MWR-D-16-0413.1>

- [45] C. L. Giacomet, A. C. V. Ramos, H. S. D. Moura, T. Z. Berra, Y. M. Alves, F. M. Delpino, J. E. Farley, N. R. Reynolds, J. B. Alonso, T. K. A. Teibo, R. A. Arcêncio, A distributional regression approach to modeling the impact of structural and intermediary social determinants on communities burdened by tuberculosis in Eastern Amazonia – Brazil, *Archives of Public Health* 81 (1) (2023) 135. doi:10.1186/s13690-023-01147-7. URL <https://doi.org/10.1186/s13690-023-01147-7>
- [46] P. Friederichs, T. L. Thorarinsdottir, Forecast verification for extreme value distributions with an application to probabilistic peak wind prediction, *Environmetrics* 23 (7) (2012) 579–594. doi:10.1002/env.2176. URL <https://onlinelibrary.wiley.com/doi/abs/10.1002/env.2176>
- [47] R. A. Johnson, quantile-forest: A Python Package for Quantile Regression Forests, *Journal of Open Source Software* 9 (93) (2024) 5976. doi:10.21105/joss.05976. URL <https://joss.theoj.org/papers/10.21105/joss.05976>
- [48] A. J. McNeil, R. Frey, P. Embrechts, Quantitative risk management: concepts, techniques and tools, revised edition Edition, Princeton series in finance, Princeton University Press, Princeton Oxford, 2015.
- [49] J. Velthoen, C. Dombry, J.-J. Cai, S. Engelke, Gradient boosting for extreme quantile regression, arXiv:2103.00808 (Dec. 2022). doi:10.48550/arXiv.2103.00808. URL <http://arxiv.org/abs/2103.00808>
- [50] N. Gnecco, E. M. Terefe, S. Engelke, Extremal Random Forests, arXiv:2201.12865 (Jan. 2024). doi:10.48550/arXiv.2201.12865. URL <http://arxiv.org/abs/2201.12865>
- [51] J. Ciabattini, B. Chmielewski, PJM Manual 11: Energy and Ancillary Services Market Operations (Dec. 2024).
- [52] Data Miner 2. URL <https://dataminer2.pjm.com/list>
- [53] K. Hatch, PJM Manual 13: Emergency Operations (Dec. 2024).
- [54] F. Farzan, M. A. Jafari, R. Masiello, Y. Lu, Toward Optimal Day-Ahead Scheduling and Operation Control of Microgrids Under Uncertainty, *IEEE Transactions on Smart Grid* 6 (2) (2015) 499–507, conference Name: IEEE Transactions on Smart Grid. doi:10.1109/TSG.2014.2368077.
- [55] S. Bahramara, P. Sheikahmadi, A. Mazza, G. Chicco, Day-ahead self-scheduling from risk-averse microgrid operators to provide reserves and flexible ramping ancillary services, *International Journal of Electrical Power & Energy Systems* 142 (2022) 108381. doi:10.1016/j.ijepes.2022.108381.

- [56] Y. Guo, B. Ming, Q. Huang, Y. Wang, X. Zheng, W. Zhang, Risk-averse day-ahead generation scheduling of hydro-wind-photovoltaic complementary systems considering the steady requirement of power delivery, *Applied Energy* 309 (2022) 118467. doi:10.1016/j.apenergy.2021.118467.